Development of a Modular Electromyography System

Andrew J. Peterson

Thesis submitted to the Faculty of the
Virginia Polytechnic Institute and State University
in partial fulfillment of the requirements for the degree of

Master of Science
in
Electrical Engineering

Alan Asbeck, Co-Chair
Daniel J. Stilwell, Co-Chair
William T. Baumann

July 24, 2017
Blacksburg, Virginia

Keywords: Electromyography, EMG, surface EMG, EMG signals, EMG system design

Development of a Modular Electromyography System

Andrew J. Peterson

(ABSTRACT)

The design of current EMG systems focuses on specific applications. One design focuses on the use of bipolar electrodes to monitor a single muscle group. Several of these electrodes can then be used to monitor different muscles on the body simultaneously. Another design places many electrodes in an array on a limb or over a single muscle. One cannot be used for the other. Additionally the design of an EMG system must account for several sources of noise that can be orders of magnitude larger than the EMG signal itself.

The goal of this work was to design an active EMG electrode that could be used as bipolar electrodes or in an electrode array. Two electrodes were designed and tested. One design only worked in bipolar and the other did not possess the desired noise immunity. Explanations to the behavior of the electrodes are presented along with possible modifications the the electrodes to achieve the desired performance.

Development of a Modular Electromyography System

Andrew J. Peterson

(GENERAL AUDIENCE ABSTRACT)

Electromyography or EMG is the measurement of the electrical activity produced by muscles when moving or lifting. These measurements are taken by metal electrodes placed on the surface of the skin. To properly measure the electrical activity precise measurement circuits have to be used and steps have to be taken to reduce any interference.

EMG systems are typically setup in one of two layouts. The first layout is a few electrodes are used to monitor a muscle but many different muscles can be monitored simultaneously. The second is to place many electrodes that are close to each other to monitor a single muscle. In either layout there are many types of interference that can effect the data and must be accounted for in the systems design.

In this work two electrodes were designed. The goal was to produce an electrode that would function in either layout. After testing both of the electrodes it was determined that both of the electrodes work but not as well as desired. Several future steps and design modifications are presented.

To Mom, Papa, and Grammy

without whom I would not be who and where I am today.

Contents

List of Figures

List of Tables

Abbreviations

- EMG - Electromyography
- IZ - intervention zone
- sEMG -Surface Electromyography
- Ag/AgCl - Silver/Silver-Chloride
- IA - Instrumentation Amplifier
- CMRR - Common Mode Rejection Ratio
- DRL - Driven-Right-Leg
- r.t.i. - relative to input
- ECG - Electrocardiogram
- P-SIG - Net name of one of the inputs on the electrode, connects to the non-inverting input of the IA
- P-REF - Net name of one of the inputs on the electrode, connects to the inverting input of the IA
- FFC - flat flex cable

Chapter 1

Introduction

Biopotentials present a unique and rich data set for study. Biopotentials have applications ranging from medical monitoring and diagnosis to prosthetic and robotic control. EMG is the most common as it provides a diverse set of data for its relative ease of use.

There are many varieties of Electromyography (EMG) systems. One type are for hobbyists like the single channel MyoWare^{TM} from Advancer Technologies, which is inexpensive but only includes the analog hardware and is designed with the intention of using an Ardunio to sample the signal. More advanced systems, intended for research oriented applications, are sold by several vendors but share a similar construction. One such system is the wireless multichannel system Trigno^{TM} from Delsys which can be used in a variety of EMG studies. There are also the array based EMG systems such as the 96-electrode array from [1], which are typically designed for a fixed purpose. These arrays are typically wired to a large control unit and do not facilitate mobile studies.

The focus of this work was to design a more modular EMG electrode that can be incorporated into wearable systems. Through the use of commercial IC's and innovative application of flexible circuits a compact EMG was developed that can function individually or combined with other electrodes into a larger array.

Chapter 2

Background

2.1 Electromyography

EMG measures the electrical activity produced by muscles. Muscles are composed of individual fibers which contract in response to electro-chemical signals from the brain. Many muscle fibers respond to the same signal, which are collectively considered a motor unit. When a motor unit contracts it produces a propagating voltage signal called an action potential. The action potential originates in an area of the muscle fiber refered to as the intervention zone (IZ) and propagates toward the tendons [2]. The superposition of all the action potentials make up the EMG signal, which has a reported amplitude that varies but is generally 20 µV to 5 mV detected at the surface of the skin [3], [4]. The spectrum of the EMG signal is considered to be between 0-500 Hz but there have been investigations extending this frequency range out to 1000 Hz [5].

2.2 Electrodes

There are two types of EMG electrodes: needle and surface. Needle electrodes, used in intramuscular EMG, are inserted into the skin. This type has the advantage of high selectivity and can be used to target specific motor units or muscle fibers. However the use of needle

electrodes raise sanitary concerns and in general requires a laboratory setting. Surface electrodes are used in surface EMG (sEMG) and are placed on the skin. These are non-invasive, easy to use, and cleaning can be handled with a simple alcohol wipe. The drawbacks to sEMG are each electrode picks up many superimposed action potentials and suffer from an increased sensitivity to noise.

Surface electrodes can further classified into two types: wet, and dry. Wet electrodes use an electrolytic gel to reduce the skin-electrode impedance and improves signal quality. These can be reusable but are more commonly of the disposable variety. The most popular wet electrode is the disposable silver/silver-chloride (Ag/AgCl) which come in various sizes. They are easy to use as the electrode simply sticks to the subject with the cable is snapped to it. When finished, removal of the electrode is simple which is then just thrown away and minimal cleaning of the subject and system is required. However there are detractors to using wet electrodes. Close spacing of the electrodes is not possible: disposable electrodes and the snap cables are fairly large, while manual application of electrolyte could cause neighboring electrodes to short together through the electrolyte. For long term monitoring, the signal quality degrades as the electrode gel dries. The removal of the electrode and gel could be uncomfortable for the subject and cleaning, at least for the reusable electrodes, will take time [6].

Dry electrodes, in comparison, do not use an electrode gel and as a result have a higher more variable skin-electrode impedance. These are made conductive materials such as gold, silver, steel, and sintered Ag/AgCl. Due to the variable high impedance more noise can be introduced into the data. This issue can be partly addressed by buffering the signal from the electrode. In terms of signal quality, dry electrodes are comparable to wet electrodes [6].

2.3 Skin Impedance

The skin electrode impedance is one of the key factors that affects the quality of the EMG signal. Figure 2.1 shows a detailed model of the electrode-skin interface. It is encouraged, in practice, to minimize the electrode-skin impedance, which promotes the use of gel electrodes

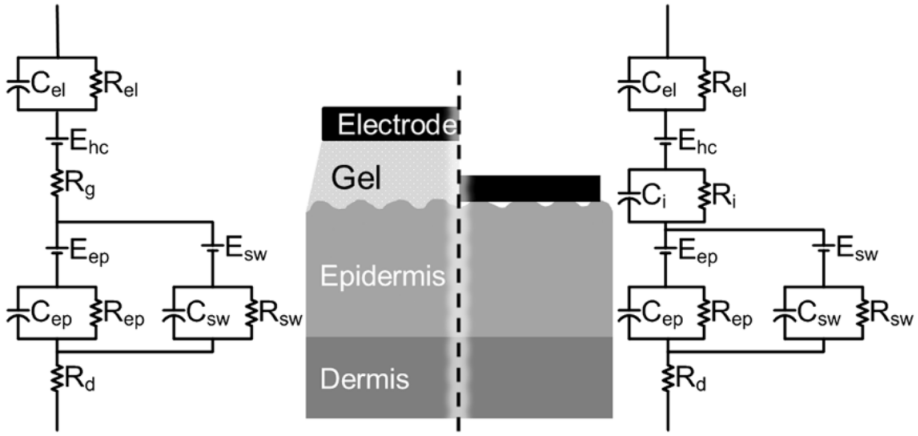

Figure 2.1: Electrode-skin interface model, taken from [7]. (Left) Model with a gel electrode. (Right) Model with a dry electrode. C_{el} and R_{el} are the capacitance and resistance of the electrode. E_{hc} is the half-cell potential. R_g is the resistance of the gel. The capacitance and resistance of the epidermis are given by C_{ep} and R_{ep}, and E_{ep} is the ionic potential between the layers of the epidermis. C_{sw} and R_{sw} are the capacitance and resistance of the sweat glands. E_{sw} is the potential produced by the current traveling through sweat. R_d is the resistance of the dermis. C_i and R_i are the capacitance and resistance of the electrode-skin interface for dry electrodes

as R_g is general much less than C_i and R_i. In the absence of gel, the presence of sweat lowers the electrode-skin impedance and serves as a lower impedance path compared to the epidermis [7].

Electrodes have an impedance that varies with frequency, as shown in Figure 2.2. The corner frequencies and impedance magnitude depend on the type and size of the electrode. Typically electrode impedances range from a few hundred kiloohms for wet electrodes to several megaohms for dry electrodes at low frequencies [8]. The impedance decreases with frequency down to several kiloohms at high frequencies.

2.4 Typical EMG System Structure

Many different EMG systems have been designed but most share a common structure. The key elements are a low-pass filter, sampling circuitry and an instrumentation amplifier (IA). The low-pass filter simply serves to prevent aliasing in the sampled signal. The instrumentation amplifier applies a gain to the inputs and then takes the difference. This is done to

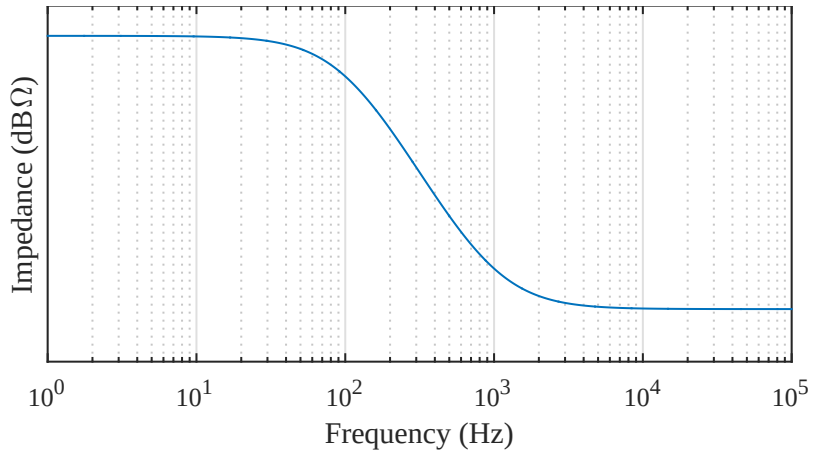

Figure 2.2: Typical electrode impedance adapted from [9]. Exacted impedances and corner frequencies vary with electrode type.

remove the common mode signal from the inputs and amplify the differential signal. It is recommended that the IA have a common mode rejection ratio (CMRR) of at least 100 dB and an input impedance above 100 MΩ to avoid loss of signal quality due to high skin impedance [8].

Additional elements that are commonly used in an EMG system include: buffers, additional gain blocks, driven-right-leg (DRL) circuit, and a high-pass filter (a more exhaustive breakdown of EMG systems can be found in [10]). The buffers are used on the inputs to help deal with impedance mismatch and noise. The DRL circuit essentially tries to driving the common mode signal to zero by feeding the negated common mode signal between two electrodes back to the subject through a third electrode which acts as a virtual ground [8]. The purpose of the high-pass filter is to remove low frequency noise in the EMG signal. It is generally considered that a high-pass filter corner frequency of 20 Hz provides a good compromise between noise rejection and signal loss [8]. De Luca et al. investigated corner frequencies from 1-40 Hz and noted that 20 Hz is generally a good choice, however the best high-pass corner frequency is dependent on the application and muscles of interest [11].

There are two configurations that can be implemented on this type of EMG system: monopolar and bipolar. In the monopolar configuration, each EMG measurement has the one electrode in common. The data from monopolar recordings are the most flexible, as any other configuration, such as the bipolar configuration and discrete Laplace filters, can be calcu-

lated from the data in software [10]. This makes monopolar more suited to EMG arrays. The bipolar configuration takes the difference between two electrodes, which are typically close together, and is more suited for use in single or multichannel EMG recording.

2.5 Noise

Due to the nature of the EMG signal and it acquisition with electrodes, there are several internal and external sources of noise that can obscure the data. These sources of noise can be several orders of magnitude greater than the EMG signal. It is therefore important to identify and reduce the effects of noise. Many methods can be found in literature with varying degrees of success. Merletti et al. provide a general characterization of the internal noise stating 1-2 μV_{rms} r.t.i. is due to the electronics and 1-4 μV_{rms} r.t.i. is due to the electrode-skin interface [10].

2.5.1 Electrode Noise

Noise is produced by the electrode-skin interface and by the circuits that condition and sample the signal. At the electrode-skin interface the ionic charge that forms on both sides of the interface produces a half-cell potential (see Figure 2.1). The half-cell potential varies widely depending on the type of metal electrode and can be on the order of volts as shown in table 2.1 [9] and can vary between electrodes of the same metal [8]. It is important that

Table 2.1: Half-cell Potentials of Common Electrode Metals [9]

Metal	Half-cell Potentials (V)
Aluminum	-1.706
Nickel	-0.230
Silver-Silver chloride	0.223
Silver	0.799
Gold	1.680

the half-cell potential be stable as variations can result in distortion of the EMG signal.

Large differences in the half-cell potential between the electrodes can cause the amplifiers to saturate. It is therefore best to use the same type of electrodes throughout the system to minimize these differences. Sometimes high-pass filters are applied to the inputs of the IA to remove the DC potential. This method runs the risk of lowering the performance as poorly matched filters will degrade the CMRR of the system. An alternative is to add a capacitor in series with the gain setting resistor of the IA as method does not affect the CMRR or the input impedance.

2.5.2 Motion Artifacts

There are three sources of motion artifacts: physical displacement of the electrode across the skin, change in skin characteristics due to deformation, and motion of the cable. The first motion artifact is due to the change in the ionic charge layer between the electrode and the skin [8]. The effects of this motion artifact are greatly reduced by using gel electrodes, which dampens the motion between the electrode and the skin. The second motion artifact is a result of the change in the geometry in the underlying skin. The ionic potentials and the resistive and capacitive properties of the skin change as the skin deforms in response to the muscle contraction. To minimize the effects of this motion artifact proper skin preparation through skin cleaning and abrasion is advised [8]. This method however raises sanitary and comfort concerns for the subject. Using an active electrode as opposed to a passive one eliminates the need for skin abrasion due to the high input impedance of the IA. A high-pass filter is also used to reduce this noise. The last motion artifact produced by the cables used to connect the electrodes to an eternal system. The movement of the cable through electric or magnetic fields can induce currents in the wire. The bending and flexing of the cable can also produce small currents [8]. The use of short shielded cables can be used to reduce the cable motion artifact. The methods used to remove the previous two motion artifacts also contribute to reducing this artifact. An active electrode provides a low impedance path to ground through the amplifier and a high pass filter attenuates the noise as it is mostly low frequency.

2.5.3 Power Line

The 60 Hz (50 Hz in Europe) power line and its harmonics are a significant source of noise and interference. The best method to reduce the effects of power line noise is distance from the source and shielding although these may not be possible in every situation. There are several ways for power line noise to appear in the EMG signal. The first is that the power line is capacitively coupled to the human body. This signal can be several orders of magnitude larger than the EMG signal. Ideally this signal is common to all electrodes and would be removed by the IA. However this is never the case due to input impedance mismatches and limited CMRR of IAs. A proposed method to reduce the power line signal on the body is by using a DRL circuit [12]. Another way the power line signal enters the is through large loops in the system. Shortening leads and minimizing loop area are the best ways to reduce this noise. Many other on-line and off-line methods have been proposed to reduce the effects of power line noise. These fit into two general categories: noise estimation and subtraction, and filtering [8]. These methods however are not widely implemented. Most assumptions made to perform noise estimation are typically not valid outside controlled situations. The filtering approach makes use of notch filters at the power line fundamental frequency. Unfortunately a significant amount of energy in the EMG signal is located around the power line frequency and is removed by the notch filter.

2.5.4 Other Sources

There are several other sources of noise that are important to note but there are few ways to correct for them. These include skin thickness, muscle crosstalk, and ECG signals. The thickness of subcutaneous fat and tissue directly affects EMG amplitude, where increasing thickness results in a decreasing amplitude [13]. Muscle crosstalk is where an EMG signal is detected from a muscle group that is near to the muscle under investigation. It has been found that crosstalk increases with subcutaneous tissue thickness [13]. The amount of crosstalk can be reduced by using small electrodes and short inter-electrode spacing [14].

The size and inter-electrode spacing use varies throughout literature. Hermens et al. found

that electrode diameters range from 1 mm to 20 mm and that the inter-electrode spacing ranges from 4 mm to 40 mm [15]. Depending on the muscle under investigation, large inter-electrode spacing could potentially could place the electrodes near the IZ or a tendon. During contraction the electrode could shift over the IZ or tendon resulting in an unstable EMG signal [16].

Chapter 3

System Design

The goal was to create a small modular active EMG electrode that could function independently or as part of a larger array containing up to one hundred. The target size of an electrode was approximately 1 cm by 1 cm. It was also desired that the electrodes function without the application of an electrode gel.

To develop an active electrode, the signal conditioning circuitry had to be fit into the 1 cm by 1 cm profile. Each electrode was designed to include sampling circuitry as well. The final design is only 1.2 cm by 1.2 cm. This was achieved by carefully placing and routing 0201 package resistors and capacitors, MSOP IC's, and 0.5 mm headers on a four-layer PCB. The final assembled PCB is shown in Figure 3.1.

3.1 Signal Processing Chain

Two implementations were developed and will be referred to as EMG 3.0 and EMG 3.1.

Each EMG reading undergoes several processing stages before being digitized. For EMG 3.0 the input signals P-SIG and P-REF, are first fed into unity-gain buffers. A gain of 300 is applied to each of the signals then P-REF is subtracted from P-SIG. The signal is then filtered by a 4^{th} order band-pass filter with a pass band of 20-1000 Hz, before being digitized.

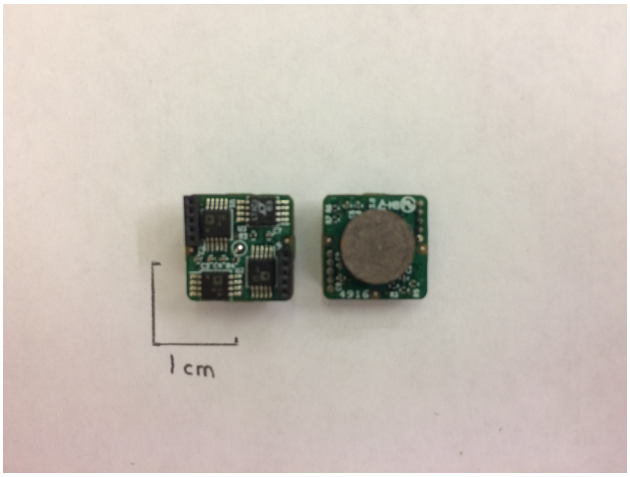

Figure 3.1: Final Electrode

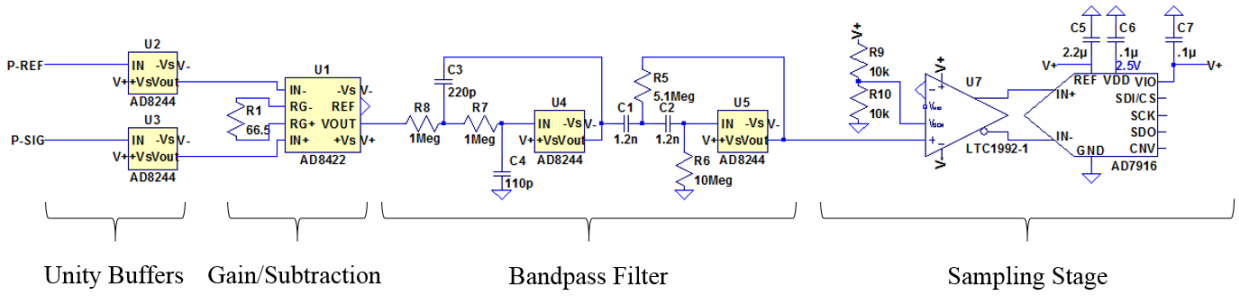

Figure 3.2: EMG 3.0 Circuit

For EMG 3.1, the signal processing chain is the same as EMG 3.0 with the addition of high-pass filters inserted between the buffered inputs and the gain stages. Each input path has a 1st order high-pass filter, with a corner frequency of 5 Hz, to remove any DC component.

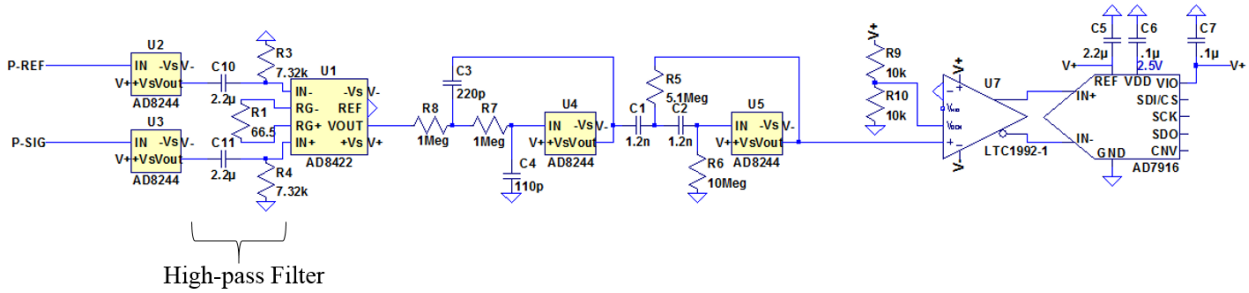

Figure 3.3: EMG 3.1 Circuit

3.2 Circuit Implementation

Each EMG electrode is a a four layer PCB. The top and bottom layers are primarily ground planes to prevent external noise from coupling into the signal traces on the inner two layers. Four IC's were used in both EMG 3.0 and EMG 3.1.

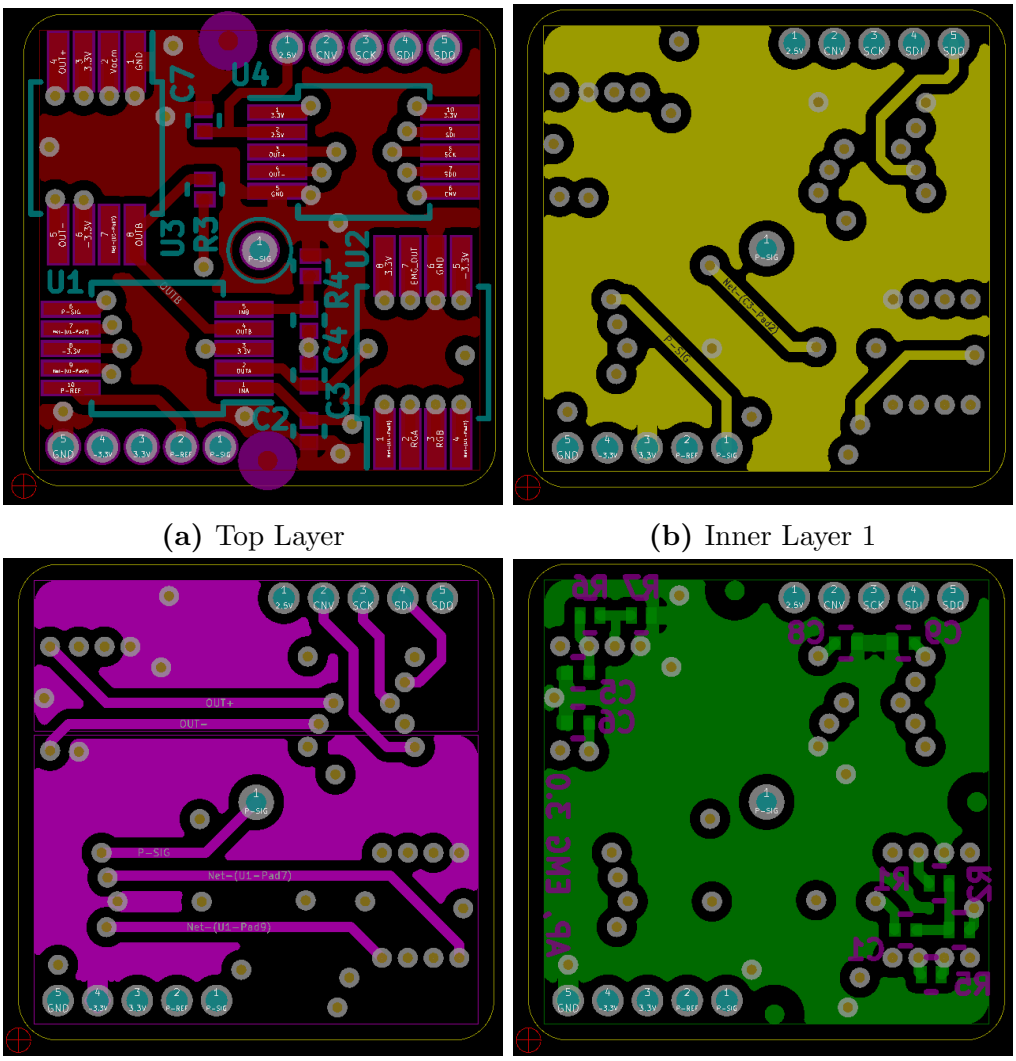

(a) Top Layer **(b)** Inner Layer 1

(c) Inner Layer 2 **(d)** Bottom Layer

Figure 3.4: EMG 3.0 board layout

The AD8244 from Analog Devices Inc. contains four 10 TΩ high impedance buffers, two of which buffer the inputs preventing any unbalance between the electrode-skin impedances from degrading the CMRR of the IA, however the buffers are only matched to 0.01% of

each other which lowers the CMRR of the system to a baseline of 80 dB. This is due to the matching error between buffers on a IC. On EMG 3.0 these input buffers were included as a precaution but may not be necessary if the impedance mismatch is less than 20 kΩ (determined through iterative simulation). These buffers are required for EMG 3.1, otherwise the input impedance of the electrode would be that of the high-pass filter. The other two buffers are used to implement the band-pass Butterworth filter using the Sallen-Key topology.

The gain and subtraction stages were implemented with the AD8422 instrumentation amplifier from Analog Devices Inc. This instrumentation amplifier was chosen for its high CMRR, high accuracy, large bandwidth, and the package size.

The digitization stage is composed of two IC's, an ADC driver and an ADC. The LTC1992-1 amplifier from Linear Technology serves as the ADC driver. The LTC1992-1 is designed to have unity gain and serves to level shift and convert the single-ended bipolar signal into a differential monopolar signal for the ADC.

The ADC chosen for the electrode was the AD7916 from Analog Devices Inc. The AD7916 is a 16-bit SAR ADC and was selected due to its maximum sample rate of 500 kHz, its SPI interface, a dedicated conversion pin, and the unique feature that it contains an internal shift register. The high sample rate means there is a short sampling time. The conversion pin allows all of the ADC's in an array to be sampled simultaneously. The internal shift register allows for multiple ADC's to be chained together on a single SPI line which reduces the total number of wires needed to connect all the electrodes to a controller. However the more electrodes that are chained together the lower the maximum sampling rate of the entire system. The maximum number of electrodes that can be supported in the system can be estimated from

$$\left\lfloor \frac{t_{sam}}{t_{clk} * 16 + t_{delay}} \right\rfloor = \text{electrodes} \tag{3.1}$$

where t_{sam} is the time in microseconds that is available to read the system, t_{clk} is the SPI bus clock period in microseconds, and t_{delay} is the conversion delay in microseconds. The ADC has a maximum conversion delay of 1.6 µs and can support a SPI clock period as short a 13 ns or clock frequency of 76.9 MHz. For this system, the SPI bus is run at 20 MHz, making

the clock period 0.05 µs and the target sampling rate of the array is 2 kHz and therefore the time between samples is 500 µs. For a single processor, it is a reasonable assumption that half of the time between samples is used for processing or storing the data. The total number of electrodes that are supported can then be found

$$\left\lfloor \frac{250}{.05 * 16 + 1.6} \right\rfloor = 104 \text{ electrodes.}$$

For the EMG 3.1 there is a simple RC high pass filter between the buffered inputs and the AD8422. This method was used opposed to adding a capacitor to the gain setting pins of the IA because of the small impedance values used use to set the gain. For example, a resistance of 66.5 Ω sets the IA to a gain of 300. To attenuated the gain of frequencies below 20 Hz the required series require capacitor would have to be 120 µF, which is not available in 0201 or 0402 packages as larger packages sizes could not be put on the board without increasing the board size.

3.3 Flexible PCB Bus

The decision to use the AD7916 allowed for an innovative design on how to interface with the array. Rather than having individual cables for each electrode as in traditional EMG systems, a modular bus connecting all of the electrodes was designed. The bus was implemented using flexible PCB's which have matching headers that mate with those on the EMG electrodes.

There are several benefits to using flexible PCB's. The biggest advantage is that flexible PCB's can be fabricated to have FFC leads. This allows the FFC and connectors can be fabricated as a single unit, reducing the overall profile of the array and allowing for a modular bus structure. Electrodes can be easily added to the system by connecting the FFC on one bus module to the connector on another. The short FFC leads eliminate the cable motion artifact present in most traditional EMG systems. The FFC allows the electrodes to flex with the muscles during contraction.

The modularity of the bus means the array is highly configurable. The shape of the bus

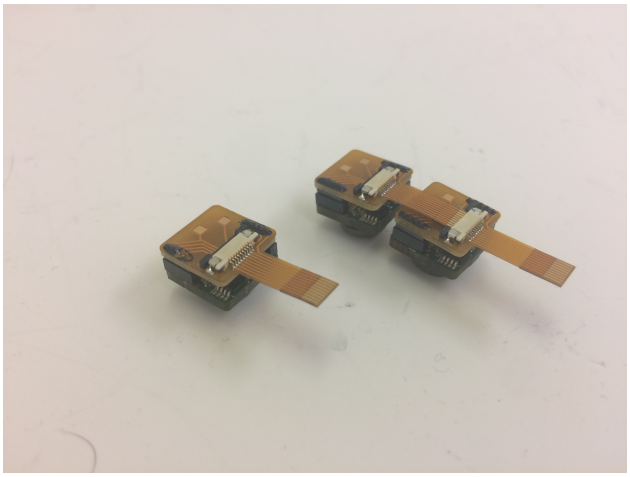

Figure 3.5: Flexible PCB and Electrode (left), Connected electrodes (right)

can be modified to accommodate different electrode layouts. Bus modules can be designed to any size and to have any number of electrodes. By changing the routing of the P-REF line on the bus the electrodes will operate as either single-ended or as differential pair. In the single-ended configuration, the P-REF signal is the same for all of the electrodes. In the differential configuration, the P-REF signal comes from the the next electrode in the array.

Since sampling occurs at the electrode site shielded cables are not necessary to preserve signal quality. This is because all but one line on the bus is either a power or digital signal line which are minimally affected by power line and RF noise. The only signal line that might be affected is P-REF and only when the bus is configured for monopolar. However P-REF is keep short enough that power line and RF noise minimally affect it as well.

The choice of controller is important as most might not be able to drive the SPI lines on large arrays. This is due to the capacitance of the bus. Using the formula for the capacitance of parallel wires the bus capacitance per centimeter can be estimated. The equation is

$$C = \frac{\pi\epsilon}{100 * \ln\left(\frac{D}{d} + \sqrt{\left(\frac{D}{d}\right)^2 - 1}\right)}$$

where ϵ is the permitivity of the polymide film, D is the distance between lines, and d is the width of the trace. Calculating the capacitance between the SPI clock line and each other line and summing the results gives approximately $3.5\,\mathrm{pF\,cm^{-1}}$. The length of the bus

modules is approximately 1.5 cm there the capacitance per bus module is approximately 5.2 pF. This means that the capacitance on the clock line would be approximately 520 pF.

3.4 Controller and Software Design

The controller can be implemented to just read and log data or it can preform some operations on the data. The current system was designed to just log the data. The chosen controller was the Raspberry Pi 2 running Ubuntu, although any device can be used so long as it implements the SPI protocol. The use of the Pi 2 simplified the process as it already has all of the necessary hardware and the software tools are readily available. All of the code was written in C.

SD cards can have long and variable write times, especially when communicating over SPI as in the Pi 2. These long write times can interfere with maintaining the desired sampling rate by forcing a single core processor to wait for the write request's completion before reading more data. There is an additional another source of indeterminate timing introduced by using the Pi 2. This is because the Pi 2 runs Linux, which makes it difficult to get real-time behavior as it is possible for the scheduler to suspend the operation of the program for other system tasks.

To counteract this, steps were taken to mitigate these effects and achieve near real-time behavior. First, three separate threads were setup: one for managing the overall operation of the program, one for reading the array, and writing the data to the SD card. Each thread was restricted to run on separate cores of the Pi 2 quad-core processor using cpusets, preventing the threads from interfering with each other. Second, to prevent the OS from suspending operation of one of the threads, each thread was run at a priority level of 98, just below the maximum. Only the most system critical operations could therefore suspend any of the threads.

The program is designed to be versatile and various configuration options can be specified as arguments in the function call. The program's main serves as the management thread.

The purpose of the management thread is to parse the input arguments, initialize the the thread communication structure, spawn the reading and writing threads, and control when the program terminates.

Communication between the threads is handled through struct emg_t to which each thread has access. The struct contains two linked lists: free_list and list_head. The free list is initialized with some number of nodes that was determined through trial and error but as the sampling rate increases the number nodes that need to be initialized also increases. Every access to emg_t is guarded by a mutex to prevent race conditions between the reading and writing threads.

The reading thread, on each sampling iteration, first reads the microsecond counter on the Pi 2 and determines the time by which the iteration should finish. This time is determined by adding the time of one sample period in microseconds to the current time and storing the result as the final time. The thread then obtains a node from free_list. If free_list is empty then a warning is printed to the screen. A significant number of warnings indicates that more nodes need to be allocated to run the array at the desired settings. The thread then signals the array to sample, waits two microseconds for the ADCs to finish sampling, then reads a number of 16-bit integers from the SPI line corresponding to the number of electrodes specified in the argument list. The data is then stored in the node which is then appended to list_head. Lastly the thread checks if it finished before the final time. If the iteration finishes before the final time, the thread simply waits until the final time before starting the next iteration. If it finishes after the final time, the amount of overrun is printed on the screen and the thread immediately starts the next iteration. If overrun occurs for a significant number of the samples or if the overrun time is large, then the number of electrodes, sample frequency, and/or clock frequency need to be adjusted. When the managing thread indicates that the program should terminate the reading thread finishes the current iteration and then terminates.

The writing thread checks if list_head has any nodes. If there is at least one node, the thread removes a node from list_head, writes the data to the file in the specified format, and then puts the node back into free_list. This process continues until list_head is empty at which

point the writing thread waits for one sample period of time before checking list_head again. When the managing thread indicates that the program should terminate, the writing thread continues to write data to the file until list_head is empty before terminating.

Chapter 4

Validation

A series of simulations and tests were performed to verify the design of EMG 3.0 and EMG 3.1. These tests included profiling tests to verify the frequency response and CMRR of the electrodes and operational tests.

4.1 Simulation

A simulation was set up in LTSpice to determine the operating range of the electrodes. The model, as shown in Figure 4.1 includes the power line noise on the skin, the impedance and half-cell parameters of the electrodes, and the EMG circuit up to the ADC driver.

Additionally the model accounts for the 0.01% gain mismatch of the high impedance buffers used to drive the inputs of the IA. This was done by adding two more of the buffers to the standard EMG circuit, one between each of the input electrodes and the normal buffer, and then adding a voltage divider to create the appropriate mismatch. The additional voltage sources after the half-cell potentials were include to simulate the mismatch in half-cell potentials.

To investigate the effects of half-cell potential mismatch on the output signal, a test EMG signal, with a maximum value of 850 µV, obtained from an initial test of EMG 3.0 was

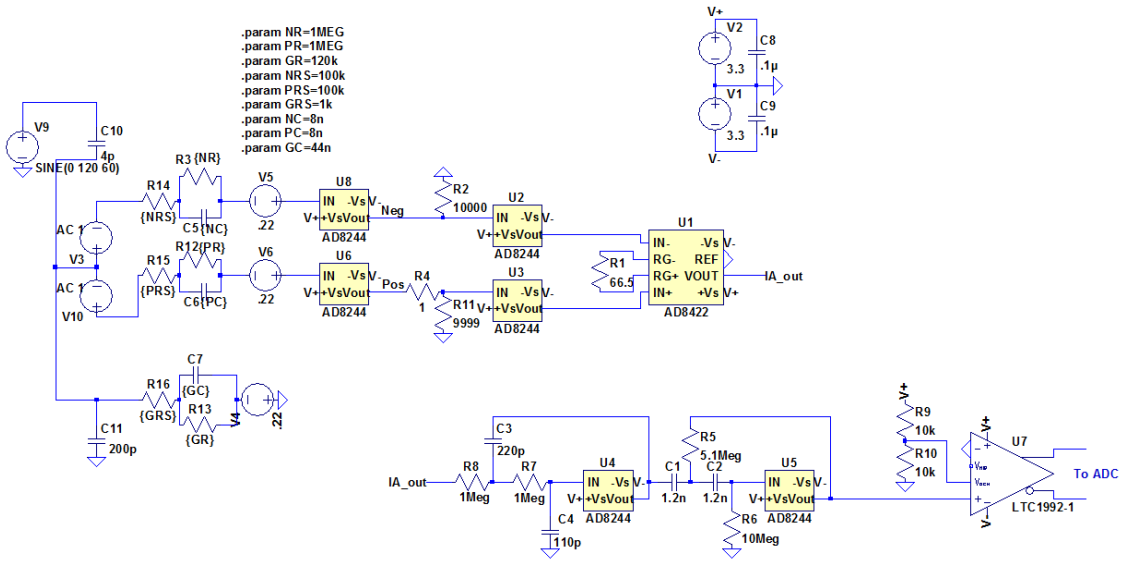

Figure 4.1: 3.0 Simulation Model

applied to the model. Then different DC offsets were applied to see how the the output signal changed. The results of four different DC offsets are shown in Figure 4.2. The results show that as the DC offset increased beyond 10 mV the amplitude of the output signal decreased. This is due to the offset driving the signal to the supply rails during the gain stage. To further investigate the effect of the DC offset the test signal was scaled to have a maximum value of 4 mV and the test repeated. The results for six DC offsets are shown in Figure 4.3. As expected smaller offsets wih the larger input signal cause output amplitude to decrease. Depending on the amount of offset and on which input the offset occurs, the output signal can experience an amplitude reduction primarily on half of the signal as in Figure 4.3c and Figure 4.3d. From these observations, a simple rule for determining the maximum tolerable half-cell mismatch potential was determined to be

$$\frac{V_{mid} - V_{min}}{G} - \min(V_{sig}) \leq DC_{off} \leq \frac{V_{max} - V_{mid}}{G} - max(V_{sig})$$

where V_{min} and V_{max} are the minimum and maximum output voltages, V_{mid} is the mid-scale output voltage, and G is the gain of the electrode. Also $\min(V_{sig}) \leq 0 \leq \max(V_{sig})$. This equation can be used to change the supplies to EMG 3.0.

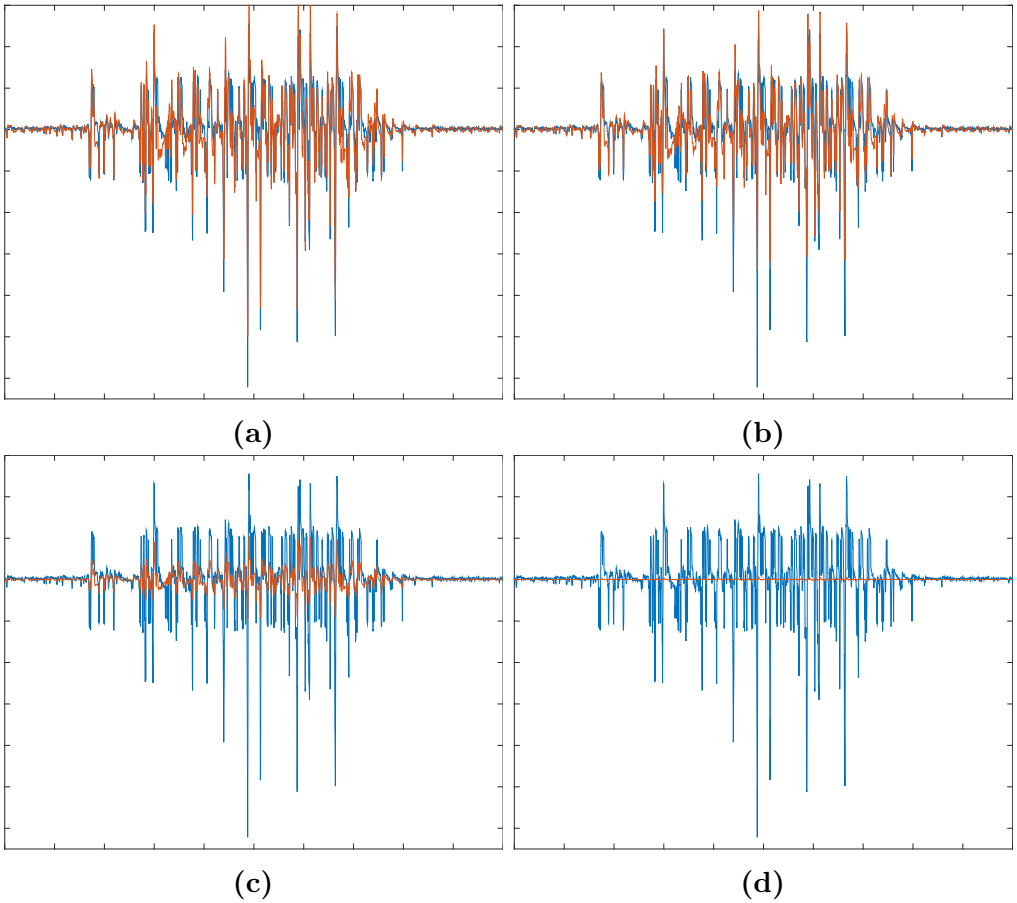

Figure 4.2: Tests with a typical EMG signal. Blue is the input signal multiplied by the gain of the system, orange is the simulated output of the system. Each of the figures represents a different offset: (a) no offset, (b) positive 10 mV offset applied to the inverting input path of the IA, (c) positive 10.5 mV applied to the inverting input path, (d) positive 11 mV applied to the non-inverting input path

4.2 Profile Tests

The test signal used to profile the electrodes was programed on a Teensy 3.2 with an output rate of 40 µs per sample. The test signal, given by (4.1), was composed of a sum of sinusoids at select frequencies between 1 Hz to 5000 Hz each with equal amplitude and was applied for 20 seconds.

$$s(t) = \sum_{j=0}^{2} \sum_{f=1}^{9} \sin(2\pi * t * f * 10^j) + \sum_{f=1}^{5} \sin(2\pi * t * f * 10^3) \tag{4.1}$$

To test the performance of the electrodes, an EMG 3.0 electrode was modified to have a gain of 1 and no band-pass filter. This was accomplished by removing the gain setting resistor,

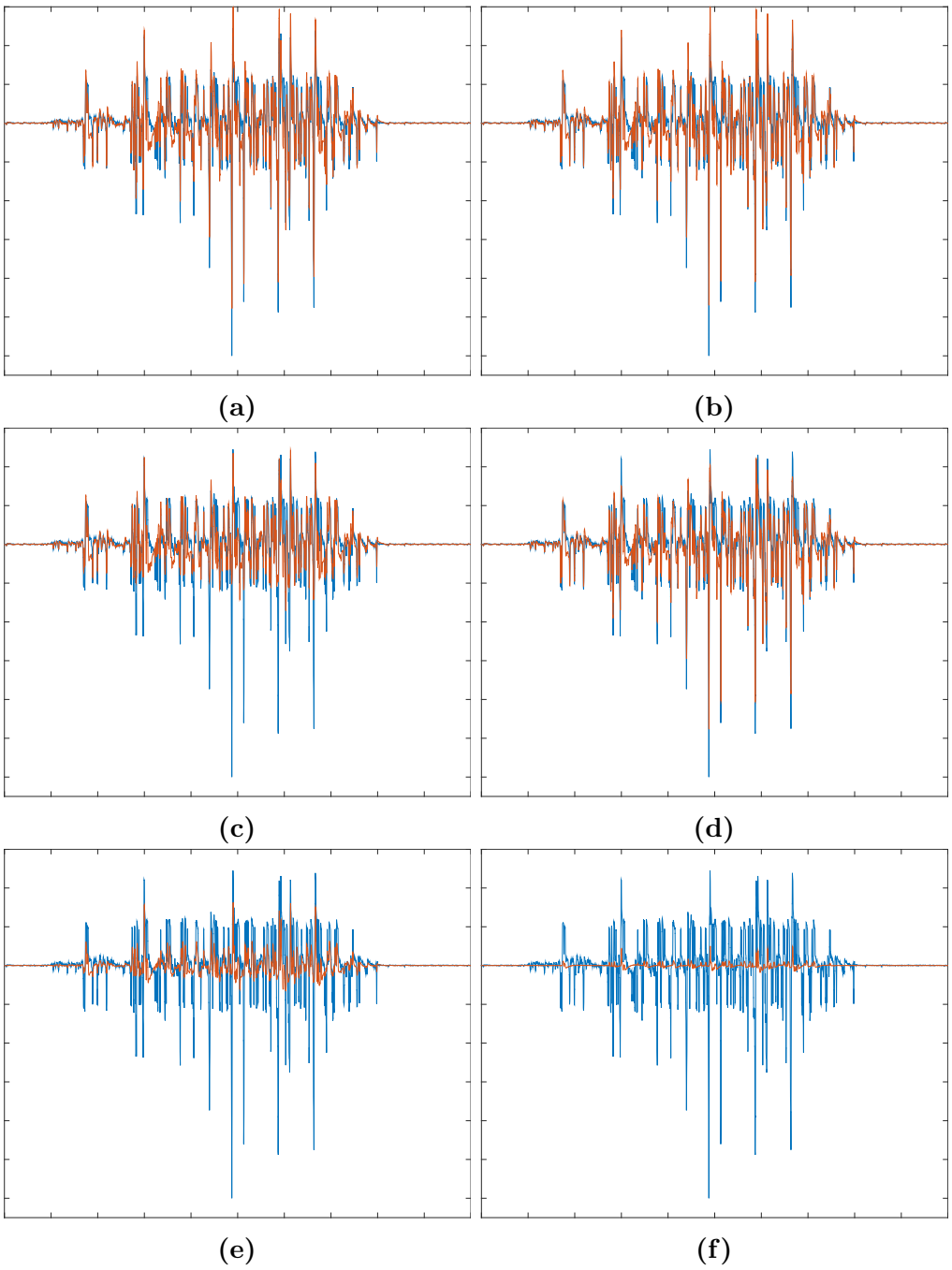

Figure 4.3: Tests with the maximized EMG signal. Blue is the input signal multiplied by the gain of the system, orange is the simulated output of the system. Each of the figures represents a different offset: (a) no offset, (b) positive 8 mV offset applied to the inverting input path of the IA, (c) positive 10 mV applied to the inverting input path, (d) positive 10 mV applied to the non-inverting input path, (e) positive 10.5 mV applied to the inverting input path, (f) positive 11 mV applied to the inverting input path

removing the filter capacitors and resistors and wiring the output of the instrumentation amplifier to the input of the ADC driver.

To verify the electrode frequency response the test signal was applied to the P-SIG input and P-REF was connected to GND on both the modified and unmodified electrodes. The data were sampled at 10 kHz and the data from the electrodes were processed using the FFT. The real and imaginary components of the FFT at the frequencies of the input sinusoids were then used to calculate the magnitude and phase of the frequency response of the electrode using the following

$$\text{mag}(f) = \frac{|F_u(f)|}{|F_m(f)|}$$
$$\text{phase}(f) = \frac{180}{\pi} * \tan^{-1}\left(\frac{Im\{F_u(f)\}}{Re\{F_u(f)\}}\right) - \frac{180}{\pi} * \tan^{-1}\left(\frac{Im\{F_m(f)\}}{Re\{F_m(f)\}}\right)$$

where $F_u(f)$ is the complex value of the FFT of the data from the unmodified electrode at a frequency f and $F_m(f)$ corresponds to the same for the modified electrode. $Re\{\bullet\}$ and $Im\{\bullet\}$ denote the real and imaginary components respectively. The results are are shown in Figure 4.4.

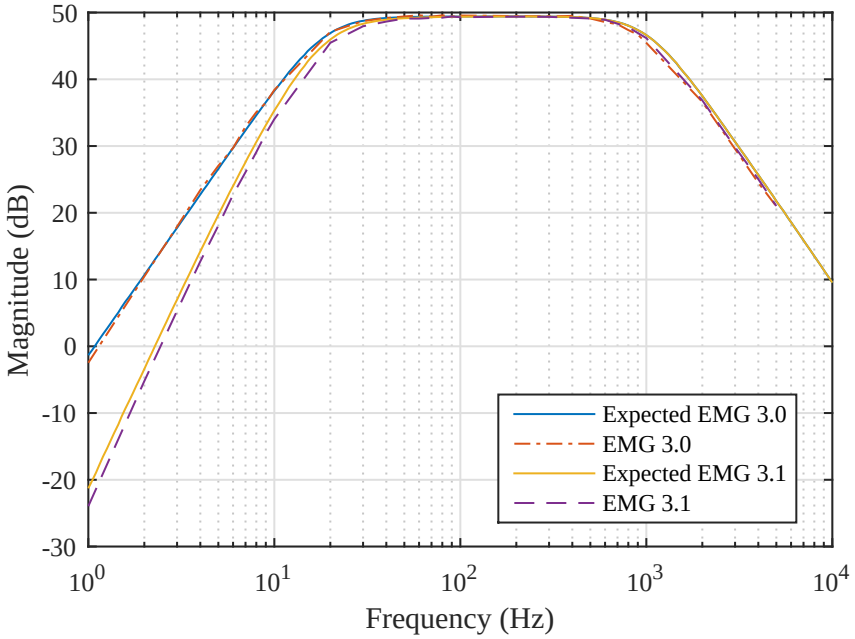

Figure 4.4: Frequency Response of the Electrodes

The CMRR was tested in a similar manner as the frequency response. To test the CMRR the modified was connected as in the frequency response test, while the unmodified electrode had the test signal applied to both P-SIG and P-REF.

$$\text{CMRR}(f) = G * \frac{|F_m(f)|}{|F_u(f)|}$$

where CMRR(f) is the CMRR at a given frequency and G is the gain of the instrumentation amplifier. As seen in Figure 4.5, the CMRR of EMG 3.1 is different from the ideal value.

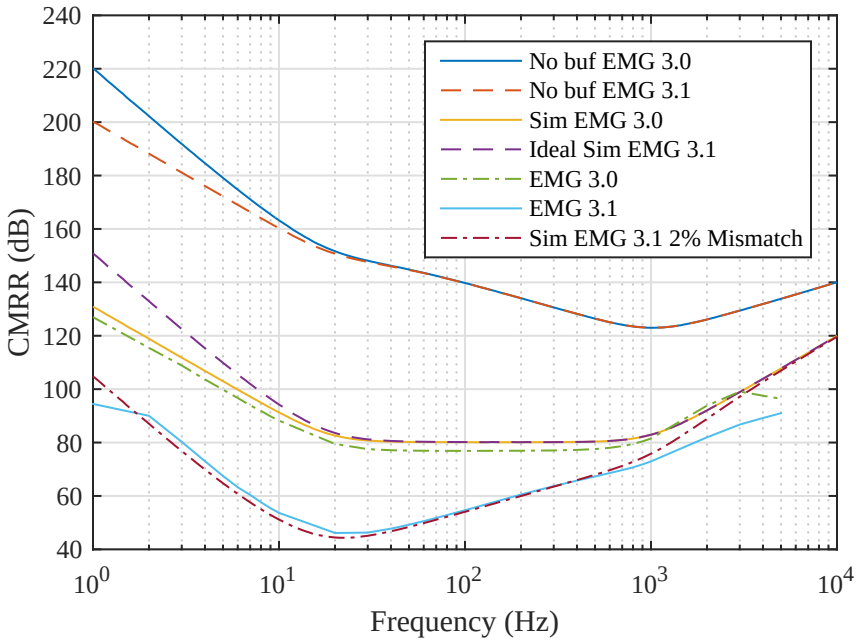

Figure 4.5: CMRR of the Electrodes

This difference is a result of the variation in the high-pass filter capacitors values by two percent from each other. This results in a mismatch in the high-pass filters which causes the common mode signals to become differential. The no buf lines represent the expected CMRR of the electrodes if the input buffers were not used.

4.3 Acquisition Tests

No abrasion or cleaning of the skin was performed. A disposable gel electrode was placed at the elbow to serve as a ground electrode. All data were collected at 2000 Hz. Over several

tests it was determined that EMG 3.0 would only work in differential configuration and that EMG 3.1 was inadequate due to the reduced CMRR.

4.3.1 Comparison Tests

To compare the performance of EMG 3.0 and EMG 3.1 a 2-by-2 array were attached to a compressive sleeve as shown in Figure 4.6. The bus connectors were modified so that each line of electrodes had a bipolar and monopolar connection. EMG 3.0, EMG 3.1, and the monopolar reference electrode used Ag/AgCl electrodes. The monopolar electrode was placed on the opposite side of the arm from the electrodes.

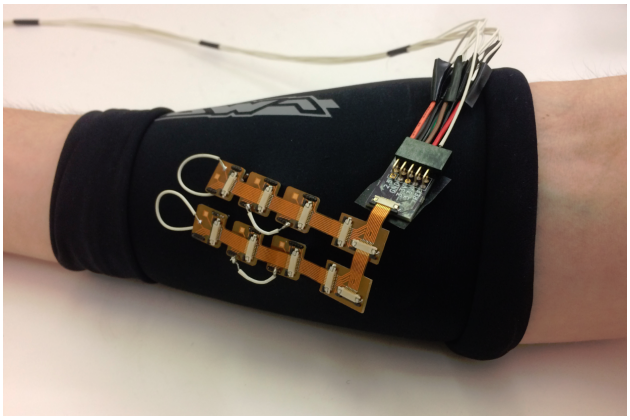

Figure 4.6: Comparison Test Setup

The data from one of the trials with this configuration is shown in Figure 4.7. The data shows that EMG 3.0 works only in differential configuration. EMG 3.1 outputs a signal in both monopolar and bipolar configuration but is corrupted by 60 Hz noise. To improve upon EMG 3.1, two updated version were made by replacing the resistors and capacitors of the high-pass filter. The resulting electrodes and a high-pass cut-off frequency of 0.007 Hz and 0.15 Hz. The goal was to move the potential mismatch far from frequencies of interest. The 0.007 Hz high-pass filter was found to be too unstable to slight changes in DC. Therefore the electrode with the 0.15 Hz was used with the configuration described above. The updated EMG 3.1 with the lower high-pass filter presents an increased CMRR of about 20 dB compared to the original EMG 3.1 but still does not offer the bipolar performance of EMG 3.0 as shown in Figure 4.8.

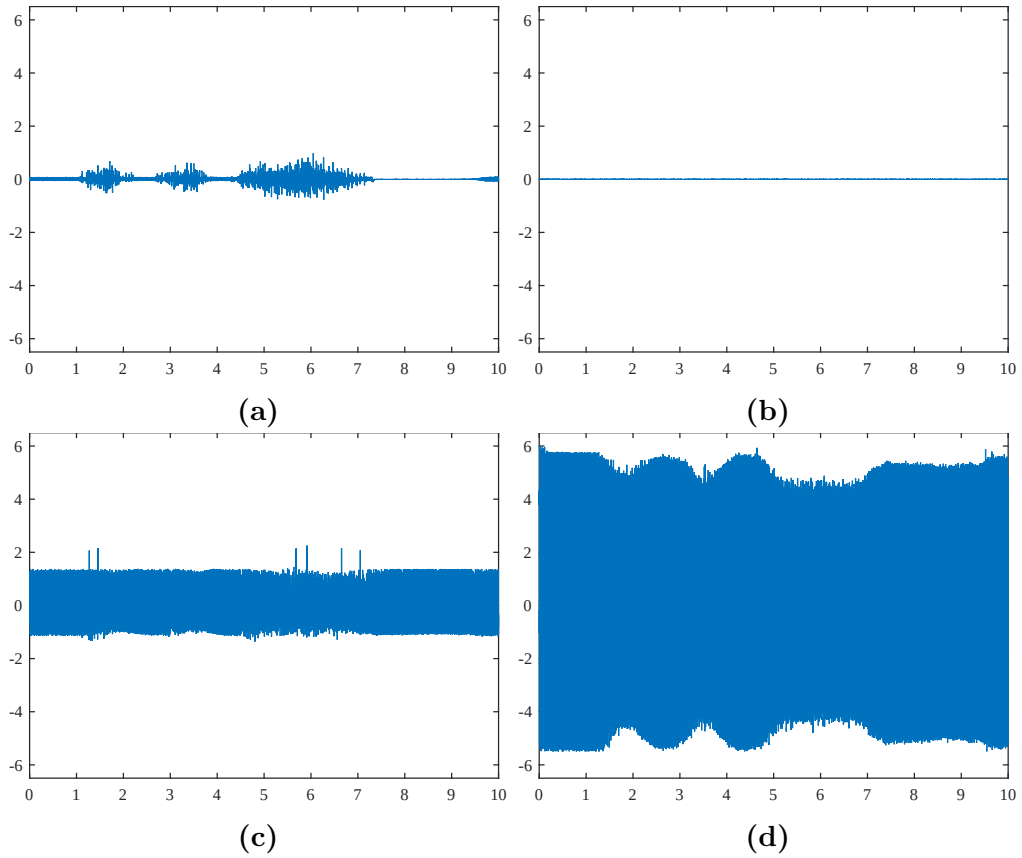

Figure 4.7: Data from EMG 3.0 and EMG 3.1. The x-axis is in seconds and the y-axis is in millivolts. (a) Bipolar EMG 3.0, (b) Monopolar EMG 3.0, (c) Bipolar EMG 3.1, (d) Monopolar EMG 3.1

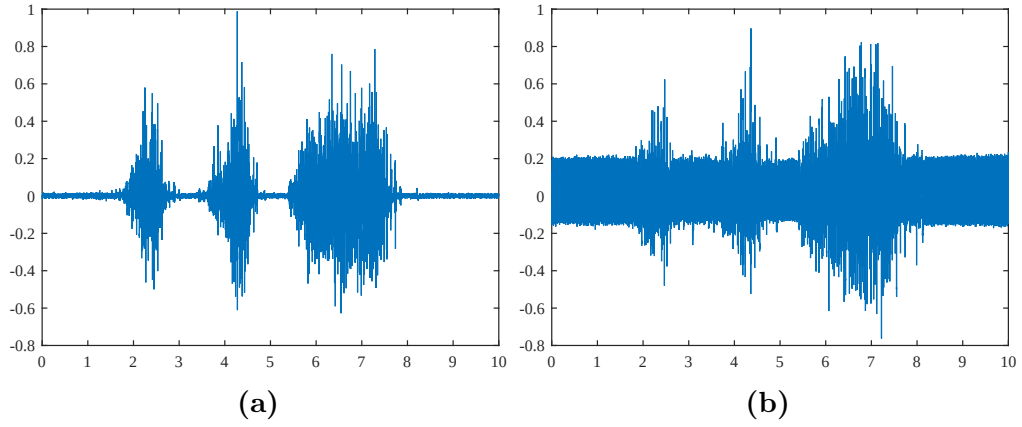

Figure 4.8: Data from EMG 3.0 and modified EMG 3.1. The x-axis is in seconds and the y-axis is in millivolts. (a) Bipolar EMG 3.0, (b) Bipolar modified EMG 3.1

To further test the updated EMG 3.1, the 2-by-2 array was reconfigured to have an EMG 3.0 in differential and two of the updated EMG 3.1 in monopolar. One of the monopolar

signals was subtracted from the other and the result was compared to the differential signal. The results are shown in Figure 4.9.

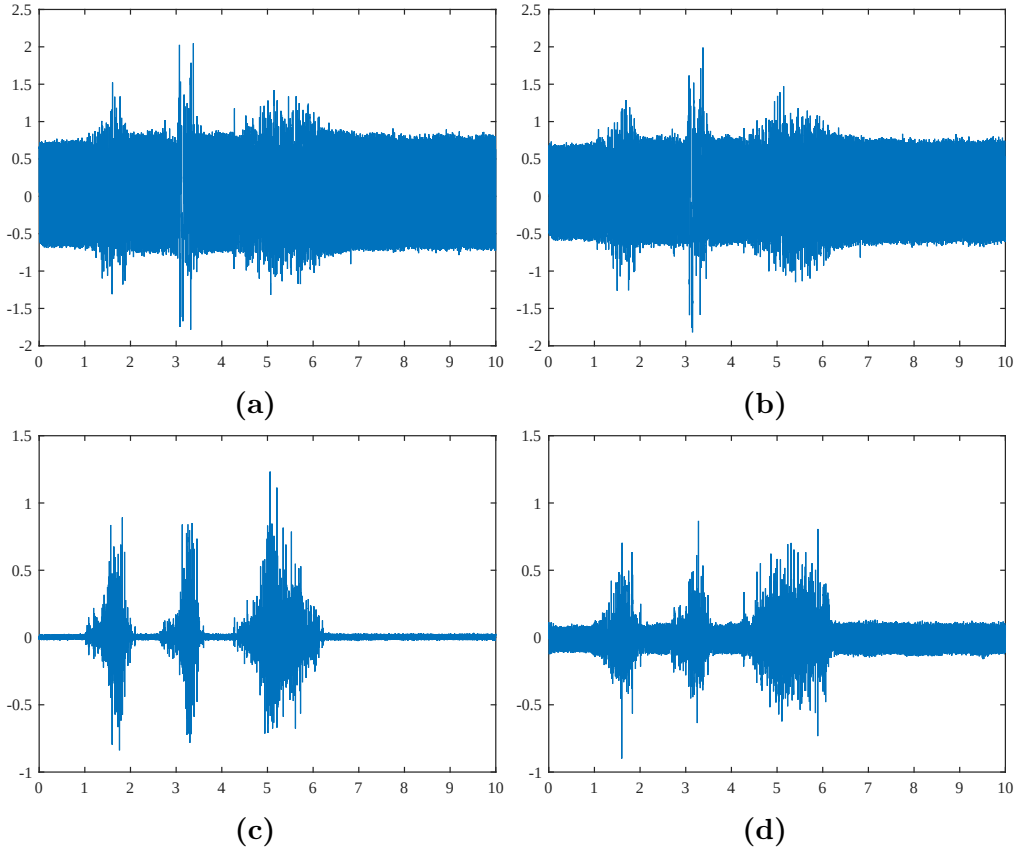

Figure 4.9: Monopolar modified EMG 3.1 recordings and EMG 3.0. (a) and (b) Monopolar modified EMG 3.1, (c) Bipolar EMG 3.0, (d) Difference of the two monopolar signals

4.3.2 Data Banding/Errors

An observation was made on several of the trials that the data seemed to be clustering into bands. This banding occurred on each electrode channel. Figure 4.10 shows the data points from several trials. It can be clearly seen that the data points cluster in bands. The middle band includes points from -64 to 63; each subsequent band consists of 128 points and is spaced 128 points from other bands.

Due to the consistency of the banding the fault is in the Raspberry Pi 2. Several tests were performed to determine the fault with the Pi 2. The first test was to determine if the Pi 2

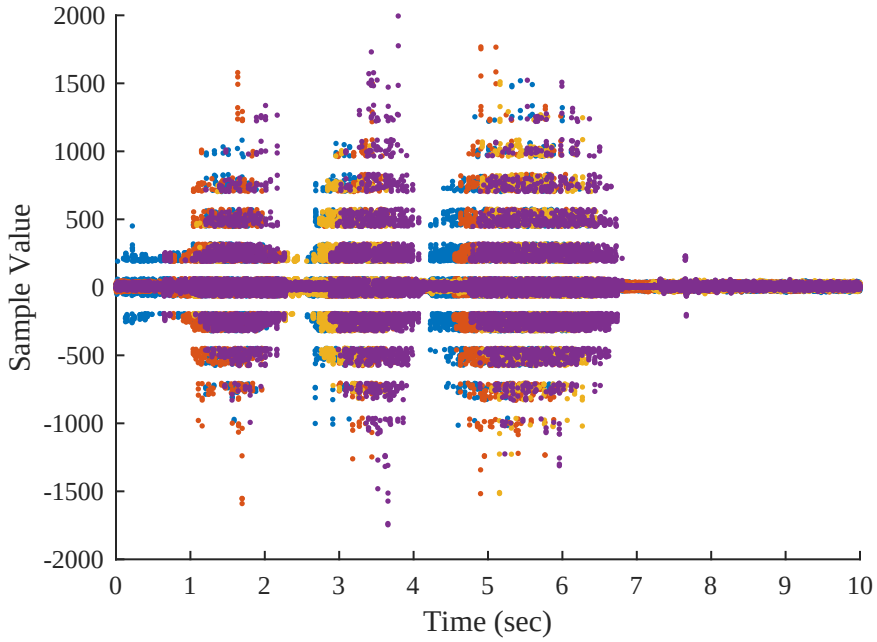

Figure 4.10: Banding Data

is unable to drive the bus lines. To test this the program was run with one more electrode than present in the array. The data for this virtual electrode would be all zero if the Pi 2 was properly driving the array. It was found that the Pi 2 was properly driving the bus with the banding of the data still present. Further tests found that lowering the SPI clock frequency from 20 MHz to 10 MHz and switching the clock phase to sample on the falling edge of the clock removed the banding effect. The results of several trials after these changes are shown in Figure 4.11. It was also discovered that the reported magnitudes were approximately half of what they should have been when the data was banding.

For a larger array the Raspberry Pi 2 is unable to drive the bus lines. This was confirmed by setting up a 5-by-5 array with a test signal applied to the last electrode. Data was read from the array as if there were 26 electrodes. The Pi 2 failed this test reporting non-zero data for the 26^{th} electrode.

To investigate why EMG 3.0 does not work in monopolar the input signals buffered and then measured by an oscilloscope. A capture of the data is show in Figure 4.12

It can be clearly seen that the magnitude of the noise and the DC offset between the inputs are significantly different. The DC offset itself is greater than 10 mV and is therefore causing

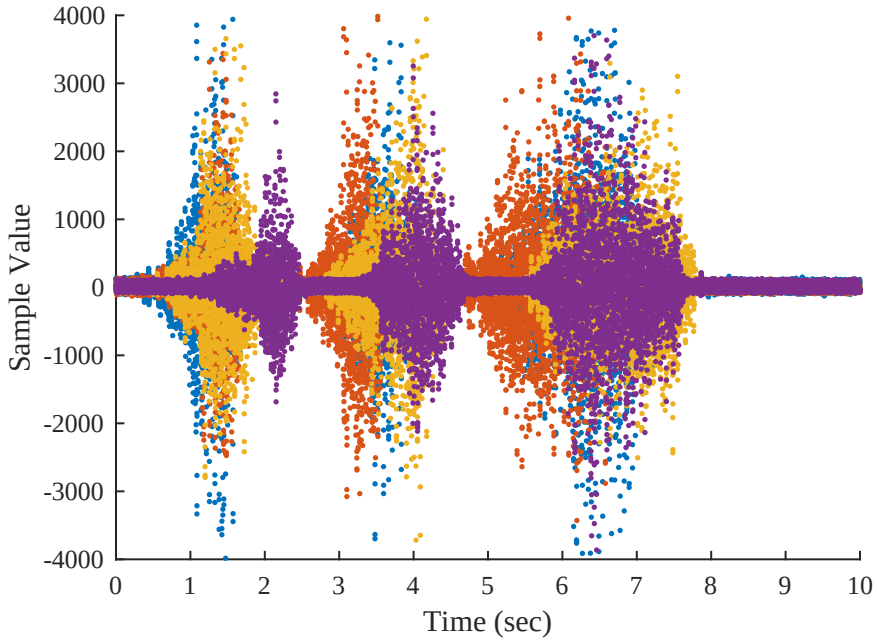

Figure 4.11: No Banding Data

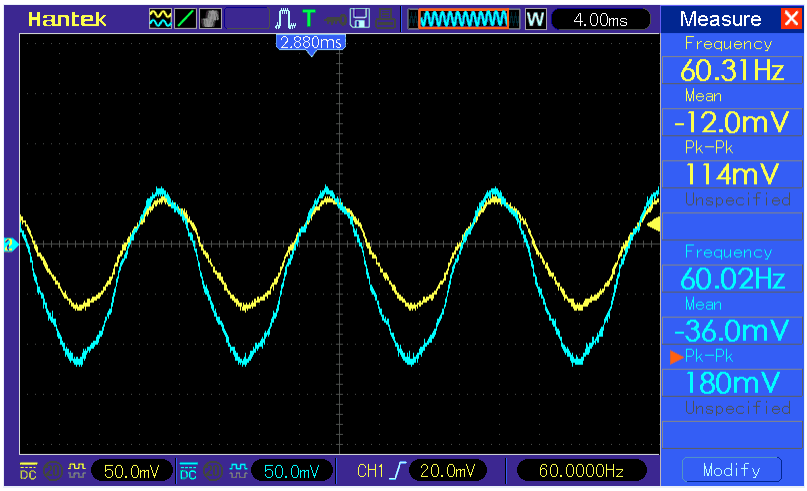

Figure 4.12: Scope Capture

the IA to hit the supplies.

Chapter 5

Conclusion

The goal of designing a modular EMG electrode has been accomplished. With additional design work the capabilities seen in EMG 3.0 and EMG 3.1 could be combined into a future design. Overall the Raspberry Pi 2 does not seem to be the best option for continued development as the capabilities to drive the bus are limited.

Table 5.1 shows a few points of comparison with this work and a commercial EMG system. It is important to note that the noise is listed as relative to input (r.t.i.). This number is obtained by dividing the noise at the output by the gain of the system. Therefore if the gain of electrodes in this work were increased to 900 then they would have have the same noise characteristics as the product from Delsys.

Table 5.1: Comparison of Available EMG Systems

Design	CMRR(dB)	Gain(V/V)	Noise(μV)[1]	Input Impedance ($\Omega \| \|$pF)	Bandwidth (Hz)
This work	≥ 78	300	≤ 3.5	$10^{13} \| \|2$	20-1000
Delsys Bagnoli^{TM} [17]	≥ 80	900	≤ 1.2	$10^{15} \| \|0.2$	20-450

[1] r.m.s., r.t.i.

5.1 Future Work

There are several avenues for future work and minor improvements.

For larger systems and higher sampling rates, larger arrays, or just more processing time between samples adding an FPGA to the data between the array and the processor is an option. Multiple SPI lines could be handled by the FPGA simultaneously and it is capable of running the SPI bus at the maximum frequency supported by the ADC. Additionally a faster interface to the processor from the FPGA would allow for a higher data throughput. Alternatively the Pi 2 could be switched out for a more faster more real-time capable processor. Despite the choice of processor a SPI bus driver might be needed to drive the capacitance on large arrays.

Another improvement would be to switch the ADC to the faster AD7915 which has half the sampling delay of the AD7916 which would increase the number of electrodes. This increase becomes more apparent as the SPI bus clock frequency increases. Using equation (3.1) on page 13 with t_{sam} equal to 250 µs the number of electrodes supported for both AD7916 and AD7915 can be found. The results are shown in Figure 5.1. This shows that switching to the

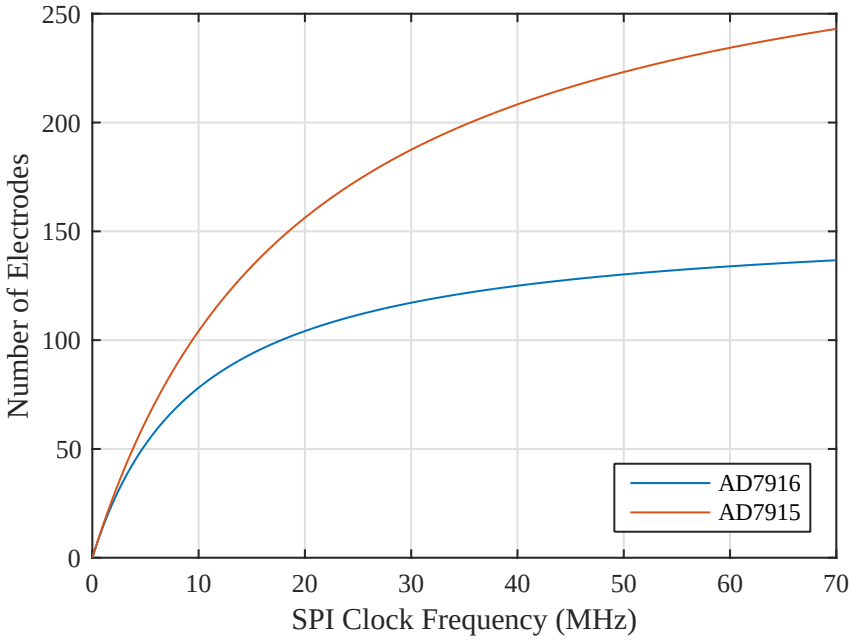

Figure 5.1: Number of electrodes supported by AD7916 and AD7915

AD7915 would be beneficial however addition circuitry would be needed to accommodate the increase in the bus capacitance from the additional electrodes.

Other potential modifications to the circuit include changing the IA so that a capacitor can be used in series with the gain resistor to remove the DC component of the signal as opposed to using high pass filter on the IA's input. This modification should then allow for the removal of the input buffers and would increase the CMRR by approximately 20 dB; this would reduce the baseline noise seen in EMG 3.0 to the noise floor. With this change the gain can also be increased. An example of this is shown in Figure 5.2. Modifying the layout

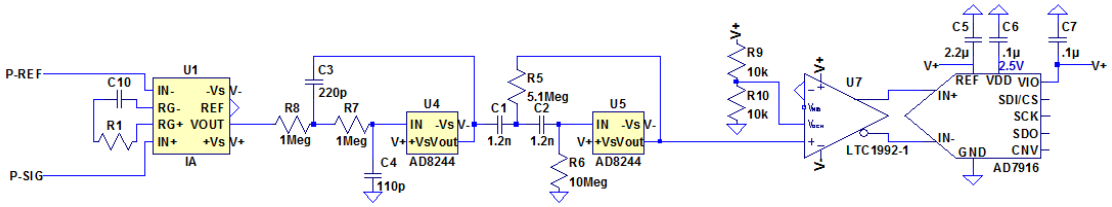

Figure 5.2: Suggested design

so that the I/O logic voltage of the ADC can be selected independent of the other supplies would also be beneficial. This would allow for the use of controllers with logic voltages other than the positive rail of the electrode. Another modification would be to convert the electrodes for single supply use, which would reduce the complexity of the power supply. It is likely that an independent bus driver will have to be included for large arrays.

Bibliography

[1] K. Nagata and K. Magatani, "Basic study on combined motion estimation using multichannel surface EMG signals.," *Conf. proc. ieee eng. med. biol. soc.*, vol. 2011, pp. 7865–8, 2011.

[2] M. Barbero, R. Merletti, and A. Rainoldi, *Atlas of Muscle Innervation Zones*. Milano: Springer Milan, 2012.

[3] G. De Luca, "Fundamental Concepts in EMG Signal Acquisition," DelSys Inc, Tech. Rep. March, 2003, pp. 1–31.

[4] A. Cohen, "Biomedical Signals: Origin and Dynamic Characteristics; Frequency-Domain Analysis," in *Biomed. eng. handb. second ed.* J. D. Bronzino, Ed., Boca Raton: CRC Press LLC, 2000, ch. 52.

[5] J. R. Potvin and S. H. M. Brown, "Less is more: High pass filtering, to remove up to 99% of the surface EMG signal power, improves EMG-based biceps brachii muscle force estimates," *J. electromyogr. kinesiol.*, vol. 14, no. 3, pp. 389–399, 2004.

[6] A. Searle and L. Kirkup, "A direct comparison of wet, dry and insulating bioelectric recording electrodes," *Physiol. meas.*, vol. 21, no. 2, pp. 271–283, May 2000.

[7] A. Cömert, M. Honkala, and J. Hyttinen, "Effect of pressure and padding on motion artifact of textile electrodes.," *Biomed. eng. online*, vol. 12, p. 26, 2013.

[8] E. A. Clancy, E. L. Morin, and R. Merletti, "Sampling , noise-reduction and amplitude estimation issues in surface electromyography," *J. electromyogr. kinesiol.*, vol. 12, pp. 1–16, 2002.

[9] M. R. Neuman, "Biopotential Electrodes," in *Biomed. eng. handb. second ed.* J. D. Bronzino, Ed., Boca Raton: CRC Press LLC, 2000, ch. 48.

[10] R. Merletti, A. Botter, A. Troiano, E. Merlo, and M. Alessandro, "Technology and instrumentation for detection and conditioning of the surface electromyographic signal : State of the art," *Clin. biomech.*, vol. 24, no. 2, pp. 122–134, 2009.

[11] C. J. De Luca, L. D. Gilmore, M. Kuznetsov, and S. H. Roy, "Filtering the surface EMG signal : Movement artifact and baseline noise contamination," *J. biomchanics*, vol. 43, no. 8, pp. 1573–1579, 2010.

[12] B. B. Winter and J. G. Webster, "Driven-right-leg circuit design," *Ieee trans. biomed. eng.*, vol. BME-30, no. 1, pp. 62–66, 1983.

[13] T. A. Kuiken, M. M. Lowery, and N. S. Stoykov, "The effect of subcutaneous fat on myoelectric signal amplitude and cross-talk," *Prosthet. orthot. int.*, vol. 27, no. 1, pp. 48–54, 2003.

[14] R. Chowdhury, M. Reaz, M. Ali, A. Bakar, K. Chellappan, and T. Chang, "Surface Electromyography Signal Processing and Classification Techniques," *Sensors*, vol. 13, no. 9, pp. 12 431–12 466, 2013.

[15] H. J. Hermens, B. Freriks, C. Disselhorst-Klug, and G. Rau, "Development of recommendations for SEMG sensors and sensor placement procedures," *J. electromyogr. kinesiol.*, vol. 10, no. 5, pp. 361–374, 2000. arXiv: `S1050-6411(00)00027-4 [10.1016]`.

[16] L. Mesin, R. Merletti, and A. Rainoldi, "Surface EMG: The issue of electrode location," *J. electromyogr. kinesiol.*, vol. 19, no. 5, pp. 719–726, 2009.

[17] Delsys. (2017). Surface EMG Sensors, [Online]. Available: `http://www.delsys.com/products/desktop-emg/surface-emg-sensors/`.